Enhanced photon absorption and carrier generation in nanowire solar cells

Wei Wang,[1,2] Shaomin Wu,[3] Randy. J. Knize,[4] Kitt Reinhardt,[5] Yalin Lu,[1,4,7] and Shaochen Chen[6,*]

[1]*HeFei National Laboratory for Physical Sciences at the Microscale, University of Science and Technology of China, Anhui 230026, China*
[2]*Guotai Junan Securities Co. Ltd., No. 168 Yincheng Middle Road, Shanghai, 200120, China*
[3]*Spansion Inc., 5204 East Ben White Boulevard, Austin, Texas 78741, USA*
[4]*Laser Optics Research Center, Physics Department, United States Air Force Academy, Colorado 80840, USA*
[5]*United States Air Force Office of Scientific Research, AFOSR/NE, 875 North Randolph Street, Suite 326, Arlington, Virginia 22203, USA*
[6]*Department of NanoEngineering, Atkinson Hall, MC-0448, University of California, San Diego, 9500 Gilman Drive, La Jolla, California 92093, USA*
[7]*yllu@ustc.edu.cn*
[*]*chen168@ucsd.edu*

Abstract: Overall performance of a thin film solar cell is determined by the efficiency of converting photons to electrons through light absorption, carrier generation, and carrier collection. Recently, photon management has emerged as a powerful tool to further boost this conversion efficiency. Here we propose a novel nanograting solar cell design that achieves enhanced broadband light absorption and carrier generation in conjunction with the reduced use of active and non-earth-abundant materials. A test using this design for the short circuit current density in $CuIn_xGa_{(1-x)}Se_2$ (CIGS) thin film solar cells shows up to 250% enhancement when compared to the bare thin film cells. In addition, placing metal strips on top of the nanograting to act as the top electrode reduces the use of non-earth-abundant materials that is normally used as the transparent conducting materials. This novel solar cell design has the potential to become a new solar cell platform technology for various thin film solar cell systems.

OCIS codes: (240.6680) Surface plasmons; (350.6050) Solar energy; (310.6628) Subwavelength structures, nanostructures.

References and links

1. K. R. Catchpole and A. Polman, "Plasmonic solar cells," Opt. Express **16**(26), 21793–21800 (2008).
2. A. V. Shah, H. Schade, M. Vanecek, J. Meier, E. Vallat-Sauvain, N. Wyrsch, U. Kroll, C. Droz, and J. Bailat, "Thin-film silicon solar cell technology," Prog. Photovolt. Res. Appl. **12**(23), 113–142 (2004).
3. F. Hallermann, C. Rockstuhl, S. Fahr, G. Seifert, S. Wackerow, H. Graener, G. Plessen, and F. Lederer, "On the use of localized plasmon polaritons in solar cells," Phys. Status Solidi A **205**(12), 2844–2861 (2008).
4. P. Lalanne, J. P. Hugonin, and J. C. Rodier, "Theory of surface plasmon generation at nanoslit apertures," Phys. Rev. Lett. **95**(26), 263902 (2005).
5. C. Rockstuhl, S. Fahr, and F. Lederer, "Absorption enhancement in solar cells by localized plasmon polaritons," J. Appl. Phys. **104**(12), 123102 (2008).
6. D. M. Schaadt, B. Feng, and E. T. Yu, "Enhanced semiconductor optical absorption via surface plasmon excitation in metal nanoparticles," Appl. Phys. Lett. **86**(6), 063106 (2005).
7. S. Pillai, K. R. Catchpole, T. Trupke, and M. A. Green, "Surface plasmon enhanced silicon solar cells," J. Appl. Phys. **101**(9), 093105 (2007).
8. R. A. Pala, J. White, E. Barnard, J. Liu, and M. L. Brongersma, "Design of plasmonic thin-film solar cells with broadband absorption enhancements," Adv. Mater. (Deerfield Beach Fla.) **21**(34), 3504–3510 (2009).
9. N. C. Panoiu and R. M. Osgood, Jr., "Enhanced optical absorption for photovoltaics via excitation of waveguide and plasmon-polariton modes," Opt. Lett. **32**(19), 2825–2827 (2007).
10. D. Derkacs, S. H. Lim, P. Matheu, W. Mar, and E. T. Yu, "Improved performance of amorphous silicon solar cells via scattering from surface plasmon polaritons in nearby metallic nanoparticles," Appl. Phys. Lett. **89**(9), 093103 (2006).
11. V. E. Ferry, L. A. Sweatlock, D. Pacifici, and H. A. Atwater, "Plasmonic nanostructure design for efficient light coupling into solar cells," Nano Lett. **8**(12), 4391–4397 (2008).

#159533 - $15.00 USD Received 6 Dec 2011; revised 21 Jan 2012; accepted 23 Jan 2012; published 31 Jan 2012

12. W. Wang, S. M. Wu, K. Reinhardt, Y. L. Lu, and S. C. Chen, "Broadband light absorption enhancement in thin-film silicon solar cells," Nano Lett. **10**(6), 2012–2018 (2010).
13. K. Aydin, V. E. Ferry, R. M. Briggs, and H. A. Atwater, "Broadband polarization-independent resonant light absorption using ultrathin plasmonic super absorbers," Nat Commun. **2**, 517 (2011).
14. L. Y. Cao, J. S. White, J. S. Park, J. A. Schuller, B. M. Clemens, and M. L. Brongersma, "Engineering light absorption in semiconductor nanowire devices," Nat. Mater. **8**(8), 643–647 (2009).
15. M. D. Kelzenberg, S. W. Boettcher, J. A. Petykiewicz, D. B. Turner-Evans, M. C. Putnam, E. L. Warren, J. M. Spurgeon, R. M. Briggs, N. S. Lewis, and H. A. Atwater, "Enhanced absorption and carrier collection in Si wire arrays for photovoltaic applications," Nat. Mater. **9**(3), 239–244 (2010).
16. E. Garnett and P. D. Yang, "Light trapping in silicon nanowire solar cells," Nano Lett. **10**(3), 1082–1087 (2010).
17. L. Y. Cao, P. Y. Fan, A. P. Vasudev, J. S. White, Z. F. Yu, W. S. Cai, J. A. Schuller, S. H. Fan, and M. L. Brongersma, "Semiconductor nanowire optical antenna solar absorbers," Nano Lett. **10**(2), 439–445 (2010).
18. K. S. Kim, Y. Zhao, H. Jang, S. Y. Lee, J. M. Kim, K. S. Kim, J. H. Ahn, P. Kim, J. Y. Choi, and B. H. Hong, "Large-scale pattern growth of graphene films for stretchable transparent electrodes," Nature **457**(7230), 706–710 (2009).
19. I. Repins, M. A. Contreras, B. Egaas, C. DeHart, J. Scharf, C. L. Perkins, B. To, and R. Noufi, "19.9%-efficient ZnO/CdS/CuInGaSe2 solar cell with 81.2% fill factor," Prog. Photovolt. Res. Appl. **16**(3), 235–239 (2008).
20. K. Ramanathan, G. Teeter, J. C. Keane, and R. Noufi, "Properties of high-efficiency CuInGaSe2 thin film solar cells," Thin Solid Films **480–481**, 499–502 (2005).
21. R. D. Wieting, "CIS product introduction: progress and challenges," in *Ncpv Photovoltaics Program Review - Proceedings of the 15th Conference*, M. AlJassim and J. P. Thornton, eds. (1999) pp. 3–8.
22. A. Jasenek, U. Rau, K. Weinert, I. M. Kötschau, G. Hanna, G. Voorwinden, M. Powalla, H. W. Schock, and J. H. Werner, "Radiation resistance of Cu(In,Ga)Se2 solar cells under 1-MeV electron irradiation," Thin Solid Films **387**(1-2), 228–230 (2001).
23. J. Palm, V. Probst, W. Stetter, R. Toelle, S. Visbeck, H. Calwer, T. Niesen, H. Vogt, O. Hernandez, M. Wendl, and F. H. Karg, "CIGSSe thin film PV modules: from fundamental investigations to advanced performance and stability," Thin Solid Films **451–452**, 544–551 (2004).
24. N. S. Lewis, "Toward cost-effective solar energy use," Science **315**(5813), 798–801 (2007).
25. Z. Y. Fan, J. C. Ho, T. Takahashi, R. Yerushalmi, K. Takei, A. C. Ford, Y. L. Chueh, and A. Javey, "Toward the development of printable nanowire electronics and sensors," Adv. Mater. (Deerfield Beach Fla.) **21**(37), 3730–3743 (2009).
26. S. Nanomanufacturing, Chen, ed., Nanotechnology Book Series (American Scientific Publishers, Stevenson Ranch, 2009), vol. 284.
27. *COMSOL 3.3 Reference Manual*, version 3.3 ed (2005).
28. A. Lavrinenko, P. I. Borel, L. H. Frandsen, M. Thorhauge, A. Harpøth, M. Kristensen, T. Niemi, and H. M. H. Chong, "Comprehensive FDTD modelling of photonic crystal waveguide components," Opt. Express **12**(2), 234–248 (2004).
29. E. D. Palik, *Handbook of Optical Constants of Solids* (Academic, 1985).
30. M. I. Alonso, M. Garriga, C. A. D. Rincon, E. Hernandez, and M. Leon, "Optical functions of chalcopyrite $CuGaxIn_{1-x}Se_2$ alloys," Appl. Phys. A **74**, 659–664 (2002).
31. T. W. Ebbesen, H. J. Lezec, H. F. Ghaemi, T. Thio, and P. A. Wolff, "Extraordinary optical transmission through sub-wavelength hole arrays," Nature **391**(6668), 667–669 (1998).
32. Q. Cao and P. Lalanne, "Negative role of surface plasmons in the transmission of metallic gratings with very narrow slits," Phys. Rev. Lett. **88**(5), 057403 (2002).
33. P. Lalanne, J. P. Hugonin, and J. C. Rodier, "Theory of surface plasmon generation at nanoslit apertures," Phys. Rev. Lett. **95**(26), 263902 (2005).
34. H. J. Lezec and T. Thio, "Diffracted evanescent wave model for enhanced and suppressed optical transmission through subwavelength hole arrays," Opt. Express **12**(16), 3629–3651 (2004).
35. S. A. Maier, *Plasmonics: Fundamentals and Applications,* 1st. ed. (Springer, 2007).
36. B. Z. Tian, X. L. Zheng, T. J. Kempa, Y. Fang, N. F. Yu, G. H. Yu, J. L. Huang, and C. M. Lieber, "Coaxial silicon nanowires as solar cells and nanoelectronic power sources," Nature **449**(7164), 885–889 (2007).

1. Introduction

Thin film solar cell technology presents a powerful tool to tackle the world's increasing energy shortage problem. Cost and performance are major concerns when designing a thin film solar cell to provide cheap and abundant energy. A large portion of a thin film solar cell's cost comes from the use of active semiconductor and non-earth-abundant materials [1]. In addition, reducing environmental contamination and energy consumption in processing will require minimizing their use too, due to that the production process of these materials are often hazardous. Unfortunately, designing a thin film solar cell involves an inherent tradeoff in material use vs. light absorption and efficiency. For example, to realize a complete absorption over the responsive solar spectrum in an amorphous silicon (a-Si) thin film solar cell, the absorbing layer's thickness should be at least a few micrometers. However, this is unrealistic due to the increased material cost and the stronger defect-related carrier

#159533 - $15.00 USD Received 6 Dec 2011; revised 21 Jan 2012; accepted 23 Jan 2012; published 31 Jan 2012

recombination when increasing the thickness [2]. Therefore, a new thin film solar cell design, that is able to reduce the amount of active and non-earth-abundant materials, enhance and balance the full-spectrum absorption, and improve the overall conversion efficiency, would be of significant importance.

Recently, notable progress in the field of surface plasmon polaritons (SPPs) has provided a new way to trap light, drawing significant attention in the solar cell community [3–9]. Upon excitation, SPPs cause strong near-field amplitude of the incident electromagnetic (EM) field, as well as a resonantly enhanced scattering cross section (SCS). SPPs are expected to enhance light absorption because the dissipation energy is proportional to the square of the electric field (E-field). A larger E-field leads to a stronger absorption, and a stronger SCS redirects more incident photons to the absorbing layer, substantially increasing the absorbing length. Au or Ag nanoparticles and surface nanogratings have been introduced to both crystalline and amorphous Si solar cells [5–7, 10]. Common disadvantages associated with those past efforts are that resonances can only occur at certain wavelengths, and their designs involve the use of surface metallic nanostructures directly on top of solar cells, which will block a fairly large amount of incident solar photons [5, 8, 9]. Most recently, new light absorption enhancement techniques were proposed [11–13]. Such designs achieve a large, broadband and polarization-insensitive absorption enhancement. By taking advantage of effective coupling of light to planar waveguide modes, the Fabry-Perot (FP) resonance and the SPP resonance, as high as 30% absorption enhancement was testified when using these embedded nanostructures [12].

More recently, emerging research has been focused on further reducing the use of both active and non-earth abundant materials in thin film solar cell architectures [14–17]. A nanowire optical antenna absorber was proposed [17], which demonstrates the potential to enhance short circuit current using less active material. However, the absorber does not include electrodes. To reduce the use of non-earth abundant materials, options vary according to what non-earth abundant element should be used. For example, thin film solar cells use non-earth-abundant elements in two major areas, such as indium in $CuIn_xGa_{(1-x)}Se_2$ (CIGS) as an absorbing material and in indium tin oxide (ITO) as a surface electrode. Tellurium in CdTe solar cells is another example. Replacing ITO with other conductive materials such as graphene is a new trend [18], but unfortunately, very few alternatives could be found to replace the non-earth-abundant materials in the active layer. For a CIGS thin film solar cell, it has been demonstrated that its efficiency can be as high as 20% [19, 20], an efficiency very attractive to the community. More important, CIGS solar cells showed excellent long-term stability in outdoor testing [21], high radiation resistance [22], high efficiency in large area modules [23], and the great capability to be made lightweight with flexible substrates. As a result, CIGS-based solar cells have been considered as one of the most promising solar cell technologies for cost-effective and reliable power generation. Large scale implementation of the CIGS solar cells would benefit from new technologies that are able to reduce such non-earth-abundant material usage inside both the absorbing layer and the surface electrode layer without sacrificing the light absorption efficiency [24].

In this work, a new thin film solar cell design of patterning the entire thin film solar cell structure into a nanograting array is proposed (Fig. 1). A major merit of using this structure is the potential for a significant reduction of both active and non-earth abundant material usage. For example, metallic strips on top of the active nanogratings can act as surface electrodes, and eliminate the need to use common surface electrodes such as ITO. The grating structure can also offer a large percentage reduction in the total active material usage, which can be easily determined by the grating's duty cycle. Furthermore, the structure can deliver a broadband and balanced absorption enhancement and an overall efficiency enhancement by taking advantage of metallic nanowire scattering and the SPP resonance. A remarkable improvement in the short circuit current density as high as 250% is anticipated when applying this design to CIGS thin film solar cells as compared to the corresponding bare and non-grating thin film solar cells. Additionally, unlike using other electrode materials such as graphene, fabrication of such metal-semiconductor-metal nanogratings is technically feasible and compatible with standard complementary metal-oxide-semiconductor (CMOS)

#159533 - $15.00 USD Received 6 Dec 2011; revised 21 Jan 2012; accepted 23 Jan 2012; published 31 Jan 2012

technology [25, 26]. Noting that, geometric parameters of the nanograting, as well as the performance of the solar cells are controllable based on the fabrication methods. Finally, this design could be applied to many semiconductors such as a-Si, CdTe and GaAs, and will lead to a new solar cell platform technology.

2. Computation considerations

The design shown in Fig. 1 consists of a metal (thin)-semiconductor-metal (thick) structure. The through nanograting is made from the thin metallic layer side (acting as the top electrode), and their ditches stop at the thick metallic layer surface that acts as the bottom electrode. Solar light irradiates the cell from the top with transverse electric (TE) and transverse magnetic (TM) polarizations. In order to optimize the design, it is important to study the dependence of light absorption and short circuit current on the structure's geometric parameters and incident polarizations. To simplify our discussion, we fixed the top thin metallic electrode's thickness, T_1, at 20 nm, and change other structural parameters including T_2, P, W, and the absorptive materials. Here silver was selected as both top and bottom electrode material and CIGS as the absorbing material. The gap between the nanogratings was assumed to be filled with air. Absorption enhancement in the absorbing layer and the short circuit current were also calculated over different absorptive materials such as a-Si, CdTe, and GaAs, with the goal of evaluating overall performance.

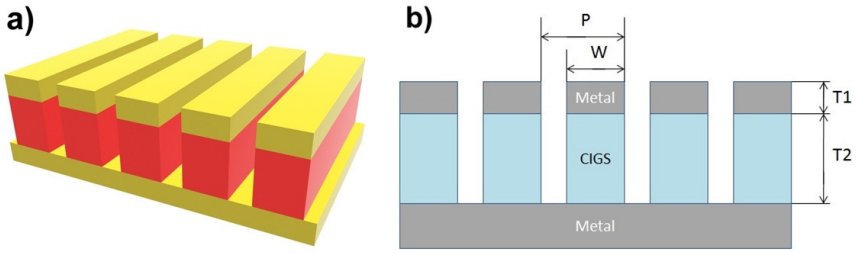

Fig. 1. The proposed solar cell structure. (a) A 3D conceptual schematic diagram. (b) A cross-sectional view outlining the device's structure to be used in the simulation. The top electrode thickness is T_1, the nanograting width is W, the period is P, and the active layer thickness is T_2.

We calculated the absorption enhancement and short circuit current by analyzing the electromagnetic (EM) field distribution across the cells. EM fields were assumed to be time harmonic and the resulting governing equations for the steady-state distribution were solved using a commercial 2-dimesnioanl finite element software (COMSOL 3.3) [27]. The computational domain considered is a single unit cell surrounded either by periodic boundary conditions or by perfectly matching layers [28]. The dispersive dielectric constants of silver and CIGS can be found in the references [29, 30]. Using the calculated EM distribution inside the cell, the absorption by the absorbing layer for an incident monochrome plane wave with certain wavelength was calculated using Eq. (1):

$$A(\lambda) = \oint_s \vec{S}(\vec{r}, \omega, \lambda) \cdot d\vec{a} \qquad (1)$$

where $\vec{S}(\vec{r}, \omega, \lambda)$ is the Poynting vector and s is the boundary of the analyzed absorptive layer.

In order to simplify the comparison, an absorption enhancement function (Λ), defined as the ratio of the absorbed energy by the nanograting solar cell over the conventional thin film solar cell with the same thickness, was used throughout our simulations. Λ is a function of the cell's geometric parameters (nanograting width, period, absorbing layer thickness, etc.), illumination conditions (incidence's wavelength and polarization), and the selected absorbing material.

#159533 - $15.00 USD Received 6 Dec 2011; revised 21 Jan 2012; accepted 23 Jan 2012; published 31 Jan 2012

3. Results

Simulation results, presented through mapping Λ with different structural parameters and incident conditions, are shown in Fig. 2. Inside those maps each point represents a full-field simulation result according to the corresponding geometric and illumination parameters. Dark red areas indicate an absorption enhancement that can reach a high level of over 3 times, referring to the side intensity bar. The absorption maps show strong and broadband enhancement within the solar spectrum, especially within the relatively long wavelength range. This unique ability to balance the absorption over the spectrum and to achieve a large and broadband enhancement is crucial. Three possible enhancement mechanisms—coupling to the multiple internal reflection resonance in the CIGS nanowire, scattering by the top silver electrode, and SPP resonance—will be discussed in details in the following sections.

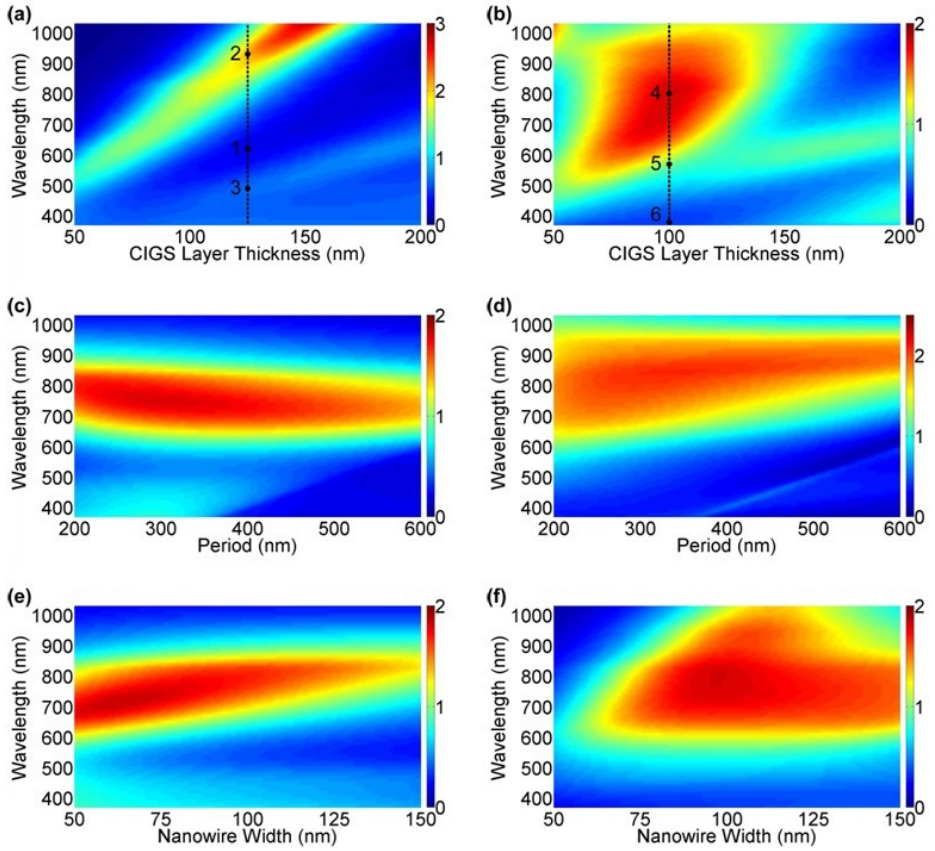

Fig. 2. Mapping the absorption enhancement with varying geometric parameters and illumination conditions. Both TE and TM polarizations were considered in order to account for the randomly polarized nature of sunlight. (a, c, e) show the case under TE illumination while (b, d, f) show TM cases. (a) and (b) show the absorption enhancement versus both wavelength and the CIGS layer thickness. The array period and wire width are 200 nm and 100 nm, respectively. (c) and (d) show the enhancement versus both wavelength and the nanowire array's period. In these cases, the CIGS nanowire layer thickness and width (W) were both fixed at 100 nm. (e) and (f) show maps of the absorption enhancement versus both wavelength and nanowire width (W). The array period and wire thickness are fixed at 200 nm and 100 nm, respectively.

3.1 Absorption enhancement mechanisms

Figures 2(a) and 2(b) shows the absorption enhancement maps vs. CIGS layer thickness inside the nanograting cell and wavelength under both TE and TM illumination. Holding the

#159533 - $15.00 USD Received 6 Dec 2011; revised 21 Jan 2012; accepted 23 Jan 2012; published 31 Jan 2012

thickness constant (denoted as dashed lines in Fig. 2), the absorption enhancement will reach several peaks and deeps when changing the incoming light wavelength. In our analysis, (EM) field across the cell structure at these peaks and deeps are plotted to study the absorption enhancement mechanisms.

In the case of the TE illumination (Fig. 2(a)) and when we select the thickness at 125 nm, there is one absorption enhancement deep, point "1", and two peaks, "2" and "3" in the wavelength range. The corresponding EM field distributions are plotted in Fig. 3. For comparison, in Fig. 3(a) the electric field distribution at the same position of Point "1" in a conventional cell (no nanogratings and with a same active layer thickness) is shown. It shows a large and high electrical field in the conventional solar cell, which is due to the Fabry-Perot resonance inside the planar CIGS cavity. Changing from the planar absorbing layer to a nanograting array will break the Fabry-Perot resonance condition, which results in decreased absorption of the nanograting cell (31.7% compared with the conventional cell at this case). As the wavelength increases, the absorption enhancement becomes stronger and it reaches a peak at 800nm (marked as the Point "2"). The corresponding electric field distribution in a nanograting cell was then shown in Fig. 3(b). This figure shows that there is a large hot spot inside the CIGS nanowire, which indicates that most scattered energy is confined and absorbed in the CIGS nanowire by multiple internal reflections from the periphery two important properties. Also in this case, reflection by the Ag top electrode is weak, which is due to the strong scattering by these metallic nanowires. This results in a strong absorption enhancement (207%). As the wavelength decreases to 490nm (the Point "3" in Fig. 2), another absorption enhancement peak appears. The corresponding electric field distribution (Fig. 3(c)) shows that, the reflection rather than scattering by the metallic top nanowires dominates. Inside the CIGS nanowire, a higher order resonance can still be seen. In this case, the absorption is relatively low compared to the conventional cell (67%). According to the above analysis, scattering by the top electrode as well as the coupling to the multiple internal reflection resonance are identified as the major contribution to the observed large absorption enhancement.

Changing the CIGS layer thickness modifies the nanograting's cross section, which results in a shift in the internal reflection resonance wavelength. In Fig. 2(a) (under TE illumination), as the CIGS layer thickness increases the absorption enhancement features a red shift and becomes broader and stronger simultaneously. Unlike the TE mode, the TM illumination would excite SPPs, which results in a broad absorption enhancement band (more than 400 nm in Fig. 2(b)). As the CIGS layer thickness further increases beyond 110 nm, this SPP related enhancement weakens. Similar to the TE condition, this SPP-related enhancement red-shifts with the thicker CIGS layer.

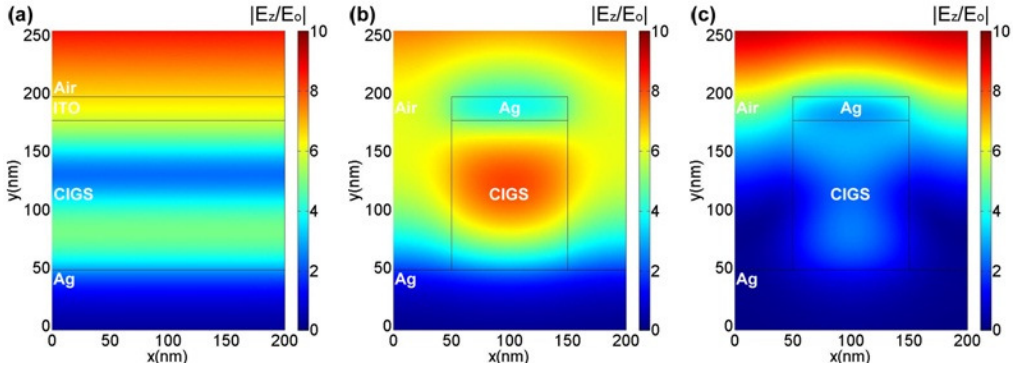

Fig. 3. Normalized and time-averaged electric field plots across the cell structure under TE illumination. In all cases, the incidence is at normal and the CIGS layer thickness is fixed at 125nm. (a) A bare CIGS layer was illuminated at wavelength of 620 nm. (b) and (c) The nanograting CIGS cells were illuminated at wavelengths of 940nm and 490nm, respectively. The period and width of the nanogratings in the latter two cases are 200nm and 100nm, respectively.

#159533 - $15.00 USD Received 6 Dec 2011; revised 21 Jan 2012; accepted 23 Jan 2012; published 31 Jan 2012

Magnetic field distribution plots across the nanograting CIGS solar cells under the TM illumination corresponding to points "4"-"6" in Fig. 2(b) were shown in Fig. 4. In this case a CIGS layer thickness of 100nm was selected (denoted as dashed line in Fig. 2(b)). We first examined the magnetic field distribution at Point "4", which is an absorption enhancement peak at the 800nm wavelength, and the results were shown in Fig. 4(a). In this case, most incoming light was transmitted through the Ag nanowire array due to the extraordinary optical transmission (EOT) phenomenon [31], which is caused by an efficient excitation of SPPs [32–34]. The transmitted light is confined in the CIGS wires which results in a strong absorption (181%) compared with the conventional cells. As the wavelength decreases, the absorption enhancement gradually attenuates, and then drops to nearly 1 where the wavelength equals 570nm (Point "5" in Fig. 2(b)). The magnetic field distribution at Point 5 was shown in Fig. 4(b). In this case the SPPs were also excited and a decent portion of the incoming light was still transmitted through the top electrode. However, most transmitted light travelled in the gaps between CIGS nanogratings and reflected back by the bottom electrode. Both the magnetic field and the absorption inside the CIGS nanogratings were lower compared to the case of Fig. 4(a). This decrease of absorption enhancement is due to: (1) more reflection by the top electrodes; and (2) more transmitted light travelling in the air gaps. As the wavelength continues to decrease, the absorption enhancement reached a trough at wavelength 380nm (Point "6" in Fig. 2(b)). The corresponding magnetic field shows that the SPPs are very weak and most incoming light was reflected by the top electrode. The magnetic fields are also very low inside the CIGS nanogratings. The absorption is thus very low compared to that of conventional cells (35%).

Changing the nanograting period will strongly affect the excited SPPs [35]. Under the TM illumination, the enhancement red-shifts as the period increases (Fig. 2(d)). At the same time, the enhancement does not change the spectral position significantly under the TE illumination (Fig. 2(c)). Similar to the CIGS layer's thickness, the nanograting width also affects the nanograting's cross section. Figure 2(e) shows that, similar to the case of changing the active layer thickness, increasing the nanograting width leads to a red-shift of the enhancement. This design is unique because the grating duty cycle (the width-over-period ratio) plays an important role in determining the absorption properties. A larger duty cycle means more used absorbing material but also more incident light to be blocked by the top metallic electrode. Figures 2(b), 2(c), and 2(d) show that as the width and period increase, both magnitude and bandwidth of the enhancement feature first undergo an increase and then diminish beyond certain points. As a result, a trade-off by balancing these two factors is needed in order to achieve the cell's maximum performance.

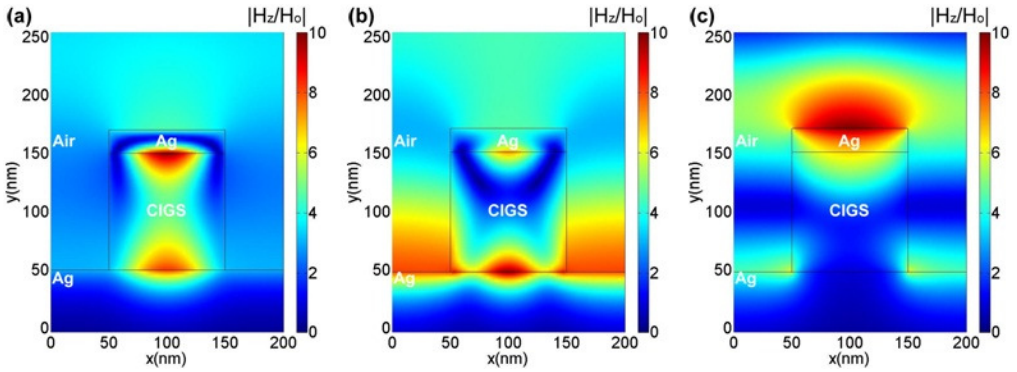

Fig. 4. Normalized and time-averaged field plots across the nanograting CIGS cells under TM illumination. In all cases, the incidence is normal and the CIGS layer thickness, period, and wire widths are 100nm 200nm, and 100nm. The wavelengths of the incoming light are 800nm, 540nm and 380nm, respectively.

#159533 - $15.00 USD Received 6 Dec 2011; revised 21 Jan 2012; accepted 23 Jan 2012; published 31 Jan 2012

3.2 Overall performance

To perform a full evaluation on the design, short-circuit photocurrent density enhancement of the nanograting solar cells must be considered. The short-circuit photocurrent of a solar cell can be calculated as:

$$J_{SC} = q\int F_s(\lambda)\eta(\lambda,G)QE_{\text{int}}(\lambda)d\lambda \tag{2}$$

Here, q is the charge carried by one electron; $F_s(\lambda)$ is the spectral photon flux density delivered by the sun (AM 1.5-G); $\eta(\lambda, G)$ is the photon absorption efficiency of a solar cell, $G = \{g_1, g_2, g_3,\ldots\}$ is the set of geometric parameters of the solar cell, in our research, for nanograting cells, the geometric parameters include T_2, P and W—the thickness, period, and the grating width while for conventional cells, the thickness is the only geometric parameter; $QE_{int}(\lambda)$ is the internal quantum efficiency of the absorbing material. The short-circuit photocurrent density is defined as photocurrent divided by the total volume of absorbing material used in the solar cell.

$$j_{SC} = J_{SC}\Big/V = \frac{1}{V}q\int F_s(\lambda)\eta(\lambda,G)QE_{\text{int}}(\lambda)d\lambda \tag{3}$$

where V is the volume of the absorbing materials.

Then, the short-circuit photocurrent density enhancement of the nanograting solar cell compared with a conventional cell can be defined as:

$$\begin{aligned} K &= \frac{j_{SC}^{NW}}{j_{SC}^{Con}} \\ &= \frac{V^{Con}\cdot q\int F_s(\lambda)\eta^{NW}(\lambda,T_2,P,W)QE_{\text{int}}(\lambda)d\lambda}{V^{NW}\cdot q\int F_s(\lambda)\eta^{Con}(\lambda,T_2)QE_{\text{int}}(\lambda)d\lambda} \\ &= \frac{V^{Con}}{V^{NW}}f(T_2)\int\frac{1}{2}F_s(\lambda)\eta^{Con}(\lambda,T_2)[\Lambda_{TM}(\lambda,T_2,P,W)+\Lambda_{TE}(\lambda,T_2,P,W)]QE_{\text{int}}(\lambda)d\lambda \end{aligned} \tag{4}$$

Here, the variables with superscripts *"NW"* and *"Con"* denote properties of nanograting and conventional cells, respectively; T_2, P and W are geometric parameters as defined above; in this equation $QE_{int}(\lambda)$, the internal quantum efficiency was assumed to be 100%, which has been demonstrated with NW junction devices [36]. $\Lambda_{TM}(\lambda, T_2, P, W)$ and $\Lambda_{TE}(\lambda, T_2, P, W)$ are absorption enhancement of nanograting cells under different incident polarizations; $f(T_2) = 1\Big/\int F_s(\lambda)\eta^{Con}(\lambda,T_2)QE_{\text{int}}(\lambda)d\lambda$ is a function of the absorbing layer thickness T_2 only. Equation (4) shows that the current density enhancement is a function of the geometric parameters of the nanograting array, with absorbing layer thickness T_2, nanograting width W, and array period P.

Figure 5 shows the simulation results of the current density enhancement versus different geometric parameters, and remarkably, the design in CIGS nanograting solar cell can enhance the overall current density over 250%. With the exception of the case where the nanograting width is very close to the period (in Fig. 5(c)), we can always expect a current density enhancement using any combination of geometric parameters.

#159533 - $15.00 USD Received 6 Dec 2011; revised 21 Jan 2012; accepted 23 Jan 2012; published 31 Jan 2012

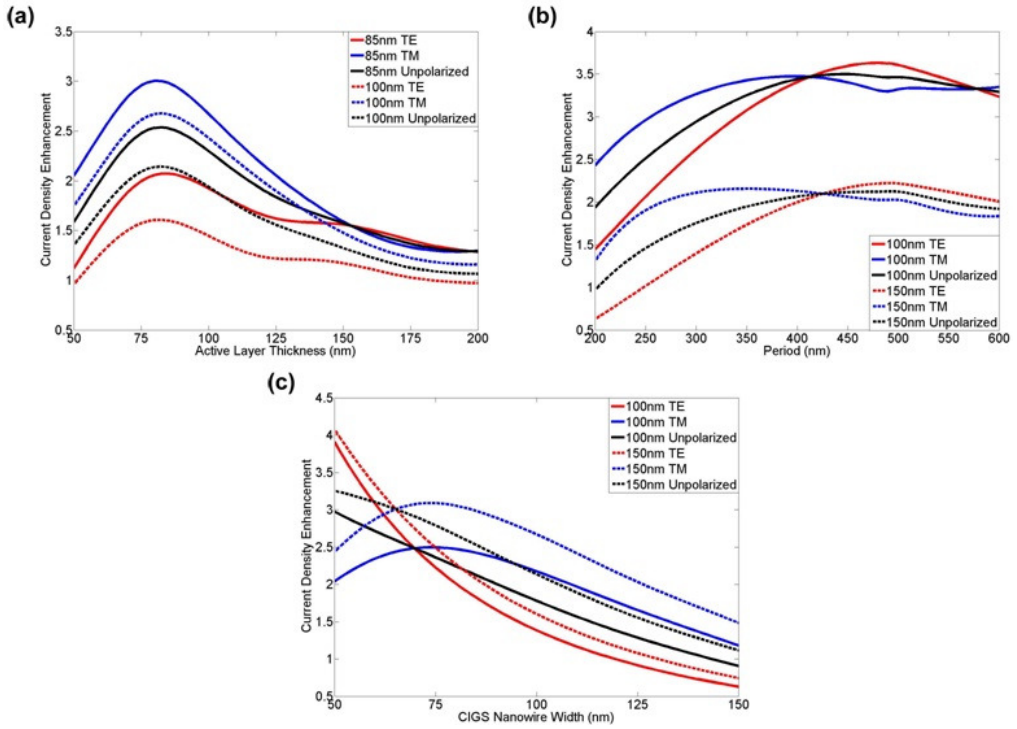

Fig. 5. Short-circuit photocurrent density enhancement over the full solar spectrum. (a-c) shows the dependency of the current density enhancement on the active layer thickness, array period, and nanograting width, respectively. (a) Current density enhancement compared with a conventional cell as a function of the active layer thickness with the array period at 200 nm, wire width at 85 nm (solid lines) and 100 nm (dashed lines), respectively. (b) Current density enhancement compared with a conventional cell as a function of array period with the wire thickness at 200 nm, wire width at 100 nm (solid lines) and 150 nm (dashed lines), respectively. (c) Current density enhancement compared with conventional cell as a function of wire width with the array period at 200 nm, wire thickness at 100 nm (solid lines) and 150 nm (dashed lines), respectively. In (a-c), red, blue and black curves show the enhancement under TE, TM and unpolarized illumination, respectively.

An alternative way to evaluate the cell's performance is to compare the total short circuit current enhancement, which is defined as the comparison of the current generated in the CIGS nanograting solar cell to the conventional cell with the same absorbing layer thickness. It is remarkable that when the nanowire width is 85 nm and the array period is 200 nm, with the CIGS thickness ranging from 70 to 95 nm, the total short circuit current generated by the CIGS nanograting solar cell can reach up to a 8% enhancement compared to its conventional counterpart, while using only 42.5% of the total absorbing material and eliminating the transparent top oxide electrode.

#159533 - $15.00 USD Received 6 Dec 2011; revised 21 Jan 2012; accepted 23 Jan 2012; published 31 Jan 2012

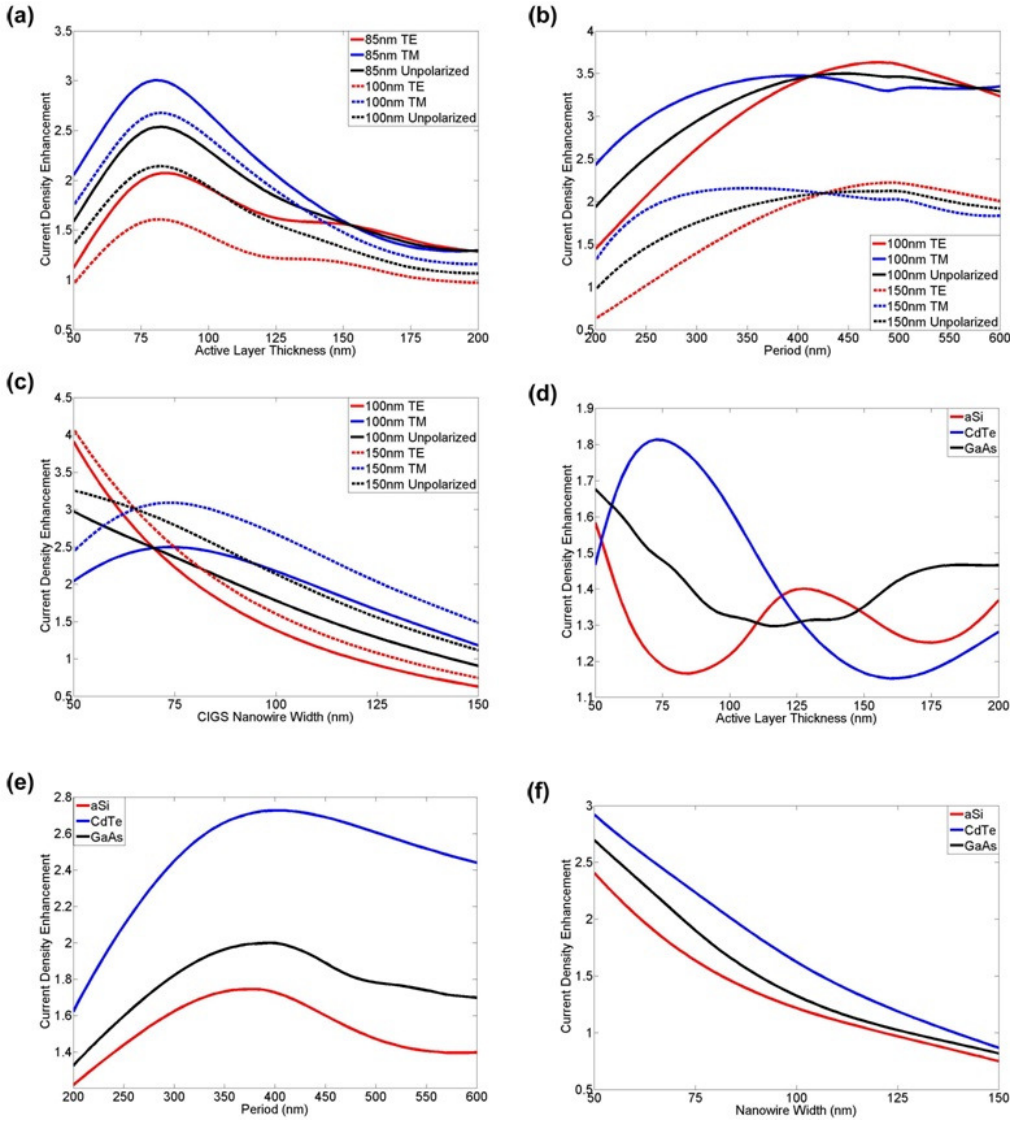

Fig. 6. Short-circuit photocurrent density enhancement over the full solar spectrum. (a-c) shows the current density enhancement dependency on active layer thickness, array period, and nanograting width, respectively. (a) Current density enhancement compared with conventional cell as a function of active layer thickness with array period at 200 nm, wire width at 85 nm (solid lines) and 100 nm (dashed lines), respectively. (b) Current density enhancement compared with conventional cell as a function of array period with wire thickness at 200 nm, wire width at 100 nm (solid lines) and 150 nm (dashed lines), respectively. (c) Current density enhancement compared with conventional cell as a function of wire width with array period at 200 nm, wire thickness at 100 nm (solid lines) and 150 nm (dashed lines), respectively. In (a-c), red, blue and black curves show the enhancement under TE, TM and unpolarized illumination, respectively. (d-f) Current density enhancement compared with conventional cell as a function of active layer thickness, period, and nanograting width. In (d), array period is 200 nm, wire width is 100 nm. In (e), active layer thickness is 100 nm, wire width is 100 nm. In (f) active layer thickness is 100 nm, array period is 200 nm. Red, blue and black curves in these figures show the enhancement using different materials (a-Si, CdTe, and GaAs, respectively).

The nanograting solar cell design was also applied to other absorbing materials, with a goal to investigate the design's potential applicability. Figure 6 shows the current density

#159533 - $15.00 USD Received 6 Dec 2011; revised 21 Jan 2012; accepted 23 Jan 2012; published 31 Jan 2012

enhancement of cells using a-Si, CdTe and GaAs. Similar to the results using CIGS, strong current density enhancements were achieved for most design geometry. Particularly within the active layer thickness range that we considered (from 50nm to 200nm), the enhancement is greater than 10% for all materials and reached 59%, 82% and 68% for a-Si, CdTe and GaAs, respectively. Such results are impressive, but they are inferior to those from the use of CIGS. The increased performance is due to better absorption (larger $\eta^{con}(\lambda)$) at long wavelength of the CIGS material. In the nanograting design, strong absorption enhancement was always observed at long wavelength (larger than 600nm). When calculating the current density enhancement by averaging the absorption enhancement over the whole solar spectrum (Eq. (4)), larger $\eta^{con}(\lambda)$ at long wavelength gave strong absorption enhancement, resulting in an enhanced current density.

3. Conclusion

The absorption of this new nanograting solar cell design is dependent on geometric parameters (layer thickness, period, and nanograting width), illumination conditions (wavelength and polarization), and construction materials (semiconductors and metals). The design is remarkable because of its ability to incorporate different absorbing mechanisms together leading to enhanced overall performance over conventional thin film solar cells. Imagine the possibility of adding a ~10% efficiency improvement over the current ~20% efficiency in CIGS thin film solar cells, using only 50% or less active CIGS materials, and using no ITO or other complicated surface electrode materials.

In conclusion, we have proposed a unique thin film solar cell design with a nanograting array as the absorbing layer. Our results show large short circuit current density enhancement compared with conventional solar cells. Moreover, this design uses no expensive and scarce transparent conducting materials. Also, this solar cell design has no critical geometry requirements, alleviating concerns associated with the high cost of complicated fabrication methods. In addition to CIGS, a similar design could be extended into other active solar materials such as *a*-Si, CdTe and GaAs, indicating the design's wide applicability.

Acknowledgments

Financial support from the US National Science Foundation (CMMI 1109591), the National Basic Research Program of China (2012CB922001), and the Air Force Office of Scientific Research (AFOSR) is greatly appreciated. The authors are grateful for the computer support from Intel's Higher Education Program.

#159533 - $15.00 USD Received 6 Dec 2011; revised 21 Jan 2012; accepted 23 Jan 2012; published 31 Jan 2012